Published in final edited form as:
Mol Cancer Res. 2013 October ; 11(10): 1223–1234. doi:10.1158/1541-7786.MCR-13-0252-T.

53BP1 is limiting for nonhomologous end-joining in ATM-deficient cells subjected to oncogenic stress or radiation

Ivana Rybanska-Spaeder[1,*], **Taylor L. Reynolds**[2,*], **Jeremy Chou**[1], **Mansi Prakash**[1], **Tameca Jefferson**[1], **David L. Huso**[3], **Stephen Desiderio**[2], and **Sonia Franco**[1]

[1]Department of Radiation Oncology and Molecular Radiation Sciences; and Department of Oncology, the Sidney Kimmel Comprehensive Cancer Center, Johns Hopkins University, 21231, Baltimore, MD, US

[2]Department of Molecular Biology and Genetics, and Institute for Cell Engineering, Johns Hopkins University, 21231, Baltimore, MD, US

[3]Department of Molecular and Comparative Pathobiology, and the Sidney Kimmel Cancer Center, Johns Hopkins University, 21231, Baltimore, MD, US

Abstract

DNA Damage Response (DDR) factors Ataxia Telangiectasia Mutated (ATM) and p53 Binding Protein 1 (53BP1) function as tumor suppressors in humans and mice, but the significance of their mutual interaction to the suppression of oncogenic translocations *in vivo* has not been investigated. To address this question, we have examined here phenotypes of mice lacking 53BP1 and ATM (*Trp53bp1*$^{-/-}$/*Atm*$^{-/-}$), relative to single mutants. These analyses reveal that loss of 53BP1 markedly decreases the latency of T lineage lymphomas driven by RAG-dependent oncogenic translocations in *Atm*$^{-/-}$ mice (average survival, 23 and 14 weeks for *Atm*$^{-/-}$ and *Trp53bp1*$^{-/-}$/*Atm*$^{-/-}$ mice, respectively). Mechanistically, 53BP1 deficiency aggravates the deleterious effect of ATM deficiency on nonhomologous end-joining (NHEJ)-mediated double-strand break (DSB) repair. Analysis of V(D)J recombinase-mediated coding joints (CJs) and signal joints (SJs) in *Trp53bp1*$^{-/-}$/*Atm*$^{-/-}$ primary thymocytes is, however, consistent with canonical NHEJ-mediated repair. Together, these findings indicate that the greater NHEJ defect in double mutants results from a decrease in the efficiency of rejoining rather than a switch to alternative NHEJ-mediated repair. Complementary analyses of irradiated primary cells indicate that defects in cell cycle checkpoints subsequently function to amplify the NHEJ defect, resulting in more frequent chromosomal breaks and translocations in double mutants cells throughout the cell cycle. Finally, we find that 53BP1 is dispensable for the formation of RAG-mediated hybrid joints (HJs) in *Atm*$^{-/-}$ thymocytes, but is required to suppress large deletions in a subset of HJs. Collectively, these results uncover novel ATM-independent functions for 53BP1 in the suppression of oncogenic translocations and in radioprotection.

Keywords

53BP1; ATM; lymphoma; translocation; double-strand break

Corresponding author: Sonia Franco, MD PhD, Department of Radiation Oncology and Molecular Radiation Sciences, Sidney Kimmel Comprehensive Cancer Center, 1550 Orleans Street, CRB II, Rm#405, Baltimore MD 21287, Phone: 410-614-9224, Fax: 410-502-2821, sfranco2@jhmi.edu.
*Both authors have contributed equally to this work

Conflict of interest statement: The authors declare no conflict of interest

Introduction

In response to DNA double-strand breaks (DSBs), mammalian cells have evolved the DNA Damage Response (DDR), a set of ubiquitous factors responsible for their detection, signaling and repair (1, 2). Upon DSB induction, the Ataxia Telangiectasia Mutated (ATM) kinase phosphorylates hundreds of substrates to promote cell cycle checkpoint activation and repair via either nonhomologous end-joining (NHEJ) or homologous recombination (HR) (3). In this context, ATM phosphorylates MDC1 to promote chromatin ubiquitination, an essential step for the recruitment of the 53BP1 adaptor to specific histone marks at sites of DSBs (4). 53BP1 in turn facilitates nonhomologous end-joining (NHEJ)-mediated repair via several mechanisms (reviewed in (5)), such as protecting broken ends from extensive end-resection (6, 7) and, in some cellular contexts, regulation of higher-order chromatin reorganization (8, 9).

Activation of the DDR represents a key barrier to cancer development (10) and, accordingly, ATM and 53BP1 are tumor suppressors in humans. Individuals with the hereditary disease Ataxia-Telangiectasia (A-T; lacking ATM) are markedly cancer prone (11). Moreover, acquired ATM mutations are frequent in B cell malignancies, where they correlate with aggressive disease and poor clinical outcome (12). Similarly, diminished 53BP1 expression is observed in lymphomas as well as solid tumors (13–17). Moreover, low levels of 53BP1 often correlate with aggressive disease (13–17) and may represent a main mechanism for acquisition of resistance to therapy in breast cancers (18).

Previous studies indicate that 53BP1 functions to concentrate activated ATM and other repair factors at sites of DSBs (19, 20). In turn, ATM-dependent phosphorylation of the 53BP1 amino terminus is essential for recruitment of Rif1 (21–24), the downstream mediator of 53BP1 in the suppression of end-resection (21–25). However, little is known on how these molecular interactions modulate the formation of chromosomal translocations *in vivo*, particularly in the context of oncogenic stress. Here, we address this question via analysis of newly generated compound mutant mice (*Trp53bp1*$^{-/-}$/*Atm*$^{-/-}$ mice).

Materials and Methods

Mice and cells

Trp53bp1$^{-/-}$ mice (26) and *Atm*$^{-/-}$ mice (27) were obtained from Drs. Junjie Chen and Fred Alt, respectively. *Trp53bp1*$^{-/-}$ mice were backcrossed into 129/Sv mice for six generations and then bred to 129/Sv *Atm*$^{-/-}$ mice to generate double mutants and all corresponding controls. All mouse experiments were conducted in accordance with Institutional Animal Care and Use Committee (IACUC)-approved protocols and following guidelines from the US Public Health *Policy on Humane Care and Use of Laboratory Animals*. Purification and *in vitro* activation of mature B and T lymphocytes was done as described (28). For irradiation experiments, mice or cells were exposed to 2 Gy of IR using a ^{137}Cs source (GammaCell40), at a rate of 0.5 Gy/min.

Immunophenotyping and cell cycle analysis

Thymocytes and splenocytes of 8–12 week-old mice were stained with antibodies to T cell or B cell markers, as described (28). For quantification of the mitotic population, cells were co-stained with an α-phospho-histone H3 (Ser10) antibody (Millipore) and propidium ioidide (PI). Data was acquired using a FACSCalibur and analyzed with FlowJo software.

Cytogenetic assays

Metaphase preparation and telomere FISH were previously described (28). For TCRα/δ locus-specific FISH, we detected the 5′ end of the locus using BAC RP23-304L21 (purchased from Children's Hospital Oakland Research Institute) and the 3′end using BAC TCR-Cα (kind gift of Dr. Carol Greider). BAC labeling, hybridization and detection were performed as described (28). Paints to mouse chromosomes 12 and 14 were purchased from Cambio (Cambridge, England) and hybridized following manufacturer's instructions. All images were acquired using a Zeiss Axioplan Imager Z.1 microscope equipped with a Zeiss AxioCam and an HXP120 mercury lamp (Jena GmbH) and dedicated software (Zeiss Axiovision Rel 4.6) (28). Spectral Karyotyping analysis was done as described (29).

Histopathology, immunohistochemistry and TUNEL assay on mouse tissues

Five-micron sections from formalin-fixed paraffin-embedded mouse organs were stained with hematoxylin and eosin (H/E) and evaluated by a veterinary pathologist (DLH). Immunostaining and detection of $TUNEL^+$ cells were done as previously described (29).

Immunoblotting

Cells were resuspended in RIPA buffer and protein transferred to PVDF membranes as described (29). Antibodies used were: p53 (Cell Signaling #; 1:1000); phospho-p53 (Ser15) (Cell Signaling #; 1:1000); KAP-1 (#; 1:1000); phospho-KAP1 (Bethyl Laboratories, 1:5000), or α-tubulin (Millipore, 1:5000).

Real time quantitative PCR (RT-PCR)

Thymocytes were resuspended in Trizol and RNA extracted following manufacturer's protocols. Two μg of RNA were reverse transcribed using RT-III (Invitrogen) and cDNA was amplified using Power Sybr® Green PCR Master Mix in a 7900HT Fast Real-Time PCR System with SDS v2.3 software. Data was analyzed using RQ Manager v1.2, all from Applied Biosystems (Carlsbad, California). Primers were: p21-F: 5′-TCCACAGCGATATCCAGACATT-3′; p21-R: 5′-ACGCGCTCCCAGACGAAGTTG-3′; Bax-F: 5′-CAGGATGCGTCCACCAAGAA-3′; Bax-R: 5′-CGTGTCCACGTCAGCAATCA-3′, Gapdh-F: 5′-CATGGCCTTCCGTGTTCCTA-3′; Gapdh-R: 5′-TGCCTGCTTCACCACCTTCT-3′.

Indirect immunofluorescence on cells and tissue cryosections

Splenocyte cytospins or 5-μm thymus cryosections were fixed in 4% paraformaldehyde (PFA) and immunofluorescence for γ-H2AX was done as described (28).

Sequencing of coding joints (CJs) and signal joints (SJs)

All analyses were done on thymus genomic DNA from 7 day-old mice. PCR, cloning, and sequencing of the Vδ5-Dδ2 SJ was performed as described (30). PCR, cloning and sequencing of the Vδ2-Jδ1 CJ was done as for the SJ analysis, using published primers (8).

Hybrid joint (HJ) analysis

For Dβ2-Vβ14 HJ analysis, the joint was first amplified using previously described primers (31) or newly designed primers equidistant from the junction. For the latter experiments, the primary reaction primers were: TCR5′Dβ2 Mus: GTGCACTCCAGAGAGTGCTCATGC and TCR 3′Vβ14 Mus: CTAGACAAAGACCATCTTGAACTATGC, with an annealing temperature of 56.8°C for 20 cycles. The secondary reaction primers were: TCR 5′Dβ2 Mus inside: GCACAGACAACAAGACAGGATGC and TCR 3′Vβ14 Mus inside: CCTTTCTCCTGGGCATGTTCTTG, with an annealing temperature of 57.4°C for 30

cycles. A portion of the *Rag1* locus was amplified from the genomic templates as a loading control, as described (30). Dβ2-Vβ14 HJ PCR products were transferred to a nylon membrane and hybridized overnight with a ^{32}P-labeled probe that recognizes sequences in the 5′ portion of Vβ14. Specific amplicons representing HJs harboring deletions were cut from the gel, purified, cloned into TOPO-pCR2.1 (Invitrogen) and sequenced.

Statistical analysis

We evaluated significance using Student's t-test on 3–5 datapoints per genotype. For analysis of survival, we used the log rank test.

Results

Trp53bp1$^{-/-}$/*Atm*$^{-/-}$ mice are viable and show no additional phenotypes in growth and development relative to *Atm*$^{-/-}$ mice

Intercrosses of *Trp53bp1*$^{+/-}$/*Atm*$^{+/-}$ mice produced *Trp53bp1*$^{-/-}$/*Atm*$^{-/-}$ mice at approximately Mendelian ratios (10/102 mice; expected=6.4; Table S1). Like *Atm*$^{-/-}$ and, to a lesser extent, *Trp53bp1*$^{-/-}$ mice, double mutants are growth retarded (Fig. S1A–B). However, the effect of the combined deficiency on growth was not additive, but comparable to the defect in *Atm*$^{-/-}$ mice (Fig. S1A–B). Similarly, the decreased cellularity and relative paucity of mature T cells observed in *Atm*$^{-/-}$ thymi and spleens were not further aggravated by concomitant 53BP1 deficiency (Fig. S1C–H). Pathology of *Trp53bp1*$^{-/-}$/*Atm*$^{-/-}$ organs revealed severe ovarian/testicular atrophy (comparable to *Atm*$^{-/-}$ mice; Fig. S1I and data not shown) and no significant alterations in the brain (not shown). Altogether, these findings suggest that 53BP1 and ATM function in mostly overlapping pathways during growth and development.

53BP1 deficiency accelerates lymphomagenesis in *Atm*$^{-/-}$ mice

Organismal development is mostly impaired in the context of deficiencies for Homologous Recombination (HR), a pathway that is dependent on ATM but not 53BP1 (28, 32). We therefore sought to investigate nonoverlapping roles for ATM and 53BP1 in a NHEJ-dependent process: V(D)J recombination in developing thymocytes. Here, Recombination Activating Gene (RAG) introduces DSBs within antigen receptor loci in the G1 phase of the cell cycle and NHEJ repairs them prior to DNA synthesis (30). In *Atm*$^{-/-}$ thymocytes, defective NHEJ leads to their aberrant rejoining to DSBs elsewhere to form chromosomal translocations (31, 33). Over time, selection for oncogenic translocations drives lymphomagenesis (33). To assess the effect of 53BP1 deficiency on this process, we first examined lymphoma proneness of *Trp53bp1*$^{-/-}$/*Atm*$^{-/-}$ and *Trp53bp1*$^{+/-}$/*Atm*$^{-/-}$ mice, relative to *Atm*$^{-/-}$ controls. Consistent with previous findings (27), 18/39 (46.1%) *Atm*$^{-/-}$ mice had succumbed at 6 months of age. Significantly, 35/38 (92.1%) *Trp53bp1*$^{-/-}$/*Atm*$^{-/-}$ mice had died at the same timepoint. Overall, average survival was 23 and 14 weeks for *Atm*$^{-/-}$ and *Trp53bp1*$^{-/-}$/*Atm*$^{-/-}$ mice, respectively (Fig. 1A; p=0.0001). In addition, 37/37 (100%) *Trp53bp1*$^{-/-}$/*Atm*$^{-/-}$ necropsies but only 27/32 (84.3%) *Atm*$^{-/-}$ necropsies revealed thymic lymphoma as the cause of death. Frequent tumor infiltrates were present in all major organs of *Trp53bp1*$^{-/-}$/*Atm*$^{-/-}$ mice at the time of death (Fig. 1B). We conclude that loss of 53BP1 markedly decreases the latency and increases the penetrance of thymic lymphomagenesis in *Atm*$^{-/-}$ mice. In contrast, the average survival of *Trp53bp1*$^{+/-}$/*Atm*$^{-/-}$ was comparable to *Atm*$^{-/-}$ mutants (25 weeks; Fig. 1A), indicating that one copy of 53BP1 is sufficient to suppress lymphomagenesis in this setting.

Atm$^{-/-}$ lymphomas originate from thymic precursors undergoing V(D)J recombination and invariably harbor clonal translocations with a breakpoint at the TCRα/δ locus in chromosome 14 (33) and amplification of upstream sequences (34). Similarly, *Trp53bp1*$^{-/-}$/

Atm$^{-/-}$ lymphoblasts were typically double positive (CD4^{+}/CD8^{+}) or, less frequently, single positive (CD4^{+} or CD8^{+}) (Table 1; Fig. 1C), lacked significant aneuploidy (Table 1, Fig. S2) and 6/6 tumors contained a clonal translocation involving chromosome 14, with 4/6 harboring a t(12,14) in over 90% of metaphases (Table 1; Fig. 1D). Moreover, hybridization with BAC probes that recognize sequences over the Cα region or immediately centromeric to the Vα region revealed "split" BAC signals and marked amplification of sequences 5′ to the TCRα/δ locus in most lymphoma cells (n=6 tumors; Fig. 1E–G; Fig. S3 for additional examples). More limited analyses by Spectral Karyotyping (SKY) confirmed these findings and revealed other co-existing clonal translocations (see Fig. S4), in line with previous analyses of *Atm*$^{-/-}$ lymphomas (33). Altogether, these findings suggest that loss of 53BP1 promotes lymphomagenesis in *Atm*$^{-/-}$ mice by accelerating the rate of formation of oncogenic translocations involving the TCRα/δ locus and possibly other loci.

Loss of 53BP1 aggravates the defect in canonical NHEJ in *Atm*$^{-/-}$ cells

Because NHEJ normally suppresses RAG-dependent translocations, the findings above strongly suggested a greater defect in NHEJ in double mutants. To evaluate this pathway in more detail, we took advantage of the fact that murine splenocytes are mostly noncycling and therefore rely on NHEJ for DSB repair. To assess the kinetics of NHEJ-mediated repair, resting wt, *Trp53bp1*$^{-/-}$, *Atm*$^{-/-}$ and *Trp53bp1*$^{-/-}$/*Atm*$^{-/-}$ splenocytes were irradiated and the number of γ-H2AX foci, that mark sites of DSBs, quantified over time. At 1 hour after IR, the number of foci was comparable across genotypes (Fig. 2A–B and data not shown), validating the use of this assay in our backgrounds. At later time-points however we observed a delay in the resolution of γ-H2AX foci in double mutants relative to *Atm*$^{-/-}$ controls, suggesting delayed DSB repair (Fig. 2A–B; n=2 independent experiments). These differences did not reflect on increased radioresistance of double mutant cells, because the viability of *Trp53bp1*$^{-/-}$/*Atm*$^{-/-}$ and *Atm*$^{-/-}$ irradiated cells was similar and, as expected, markedly increased relative to wt or *Trp53bp1*$^{-/-}$ cells (Fig. S5).

To further examine this question in a cell type more relevant to our tumor model and bypass potential artifacts associated with cell culture, we also quantified IR-induced γ-H2AX foci in thymus cryosections after allowing for *in vivo* repair (Fig. 2C). Foci analysis was done on the thymic cortex, which consists mostly of nondividing lymphocytes. Consistent with our observations in B cells, the number of γ-H2AX foci per nucleus was increased in irradiated double mutant thymocytes relative to *Atm*$^{-/-}$ controls, particularly 24 hours after IR (Fig. 2C). Altogether, these experiments indicate that loss of 53BP1 delays NHEJ-dependent repair in ATM-deficient cells in pre-replicative phases of the cell cycle, suggesting a mechanism for accelerated formation of RAG-dependent translocations.

53BP1 is thought to promote canonical, ligase IV-dependent NHEJ by providing a chromatin context that suppresses inappropriate end-resection, a molecular event that triggers alternative, error-prone end-joining (A-NHEJ) (6, 35). In the context of RAG-mediated DSBs, end-resection results in sequence alterations that can be readily identified by examining specific joints. However, sequences at two endogenous recombination junctions (the Vδ2-Jδ1 CJ (Fig. S6) and the Vδ5-Dδ2 SJ (Fig. S7)), in *Trp53bp1*$^{-/-}$/*Atm*$^{-/-}$ mice were indistinguishable from wt, suggesting that canonical ligase IV-dependent NHEJ remains the predominant pathway in double mutants (see Fig. S8 for the distribution of deletion size at coding and signal ends across genotypes). Specifically, we did not observe an increase in the frequency of microhomologies (MH), a footprint of alternative NHEJ (35), nor did we observe templated additions associated with products of mistimed V(D)J recombination (30) or with some oncogenic chromosomal translocations (36). We noted only rare deletions, consistent with previous observations in 53BP1-deficient cells (8).

Severe defect in p53 activation in *Trp53bp1*$^{-/-}$/*Atm*$^{-/-}$ thymocytes

In lymphoid cells, unrepaired DSBs in G1 elicit p53 activation to regulate the G1/S checkpoint and growth arrest/apoptosis. p53 activation is severely compromised in *Atm*$^{-/-}$ primary thymocytes, allowing for replication of G1-induced DSBs (37). To investigate an effect of 53BP1 deficiency on the ATM/p53 axis, we monitored IR-induced p53 stabilization and effector functions in double mutant and control thymocytes (Fig. 3). As expected, IR-induced p53 stabilization and phospho-p53 (Ser15) formation were robust in irradiated wt and *Trp53bp1*$^{-/-}$ cells, but markedly attenuated in *Atm*$^{-/-}$ thymocytes (Fig. 3A–B). A similar defect was observed in double mutants, regardless of whether radiation was administered *in vitro* (Fig. 3A) or *in vivo* (Fig. 3B). IR-dependent phosphorylation of KAP-1, another posttranslational modification primarily dependent on ATM, was also compromised to a comparable extent in *Atm*$^{-/-}$ and *Trp53bp1*$^{-/-}$/*Atm*$^{-/-}$ cells (Fig. 3A–B). As for *Atm*$^{-/-}$ cells (38), residual p53 activation and KAP-1 phosphorylation in double mutants was dependent on DNA-PKcs, because it was abrogated by pretreatment with the DNA-PKcs inhibitor NU7026 (Fig. 3C). Finally, IR-induced transcriptional activation of two main p53 targets, p21 and Bax, and thymocyte apoptosis were also attenuated to a similar extent in *Atm*$^{-/-}$ and *Trp53bp1*$^{-/-}$/*Atm*$^{-/-}$ cells (Fig. 3D–F). Collectively, these experiments indicate that double mutant cells show a severe defect in p53 activation, providing a mechanism for amplification of their increased NHEJ defect.

53BP1 is dispensable for ATM-dependent repair of replication-associated DSBs

In addition to regulating the repair of pre-replicative DSBs, ATM promotes the signaling and repair of replicative DSBs. To assess an effect of 53BP1 in this context, we next examined the kinetics of DSB repair in mature *in vitro* activated B cells (Fig. 4). We previously showed that B cell activation with α-CD40/IL-4 counteracts p53 activation in response to spontaneous DSBs (39). Consistent with those findings and a recent report (23), activated wt B cells exposed to IR (2 Gy) did not undergo significant G1/S arrest or apoptosis, but rather a transient arrest in G2 (Fig. S9). This was determined by the accumulation of cells with 4N DNA content that were also negative for the mitotic marker phospho-H3 (Ser10). In wt cells, the G2 arrest peaked by 6 hours post-IR and was resolved by 24 hours post-IR (Fig. S9). In contrast, all single and double mutants showed persistent arrest at 24 hours (n=5 independent experiments; Fig. 4A–B; Fig. S9). Significantly, double mutants consistently showed further delayed cell cycle kinetics relative to *Atm*$^{-/-}$ cells (Fig. 4A–B; Fig. S9), correlating with increased number of γ-H2AX foci at the same time-points (Fig. 4C–D). Finally, these analyses revealed that, upon irradiation, a subset of *Trp53bp1*$^{-/-}$/*Atm*$^{-/-}$ and, to a lesser extent, *Atm*$^{-/-}$ and *Trp53bp1*$^{-/-}$ activated B cells undergo a second round of inappropriate synthesis, resulting in the formation of tetraploid (8N) cells (Fig. 4E–F). The greater frequency of cells with DNA content greater than 4N in double mutants is consistent with their greater load of DSBs (Fig. 4C–D) and suggests an additional mechanism for increased genomic instability (40).

The increased load of DSBs in G2 likely result from “carry-over” of G1 breaks as well as deficient repair of newly introduced DSBs during replication. To determine whether 53BP1 may also modulate genomic instability associated with replication in *Atm*$^{-/-}$ cells, we examined genomic stability in metaphase spreads of activated B cells treated with the PARP inhibitor olaparib (Fig. S10). As expected (41), olaparib induced frequent chromatid breaks in α-CD40/IL-4-activated *Atm*$^{-/-}$ cells. 53BP1 status had no measurable effect on this phenotype, suggesting that 53BP1 aggravates DSB repair in ATM-deficient cells specifically in the context of NHEJ. These findings are consistent with our previous observations that mice lacking 53BP1 and PARP1 lack additional phenotypes (28). In further support of this notion, the frequency of hydroxyurea (HU)-induced DSBs was also comparable in *Atm*$^{-/-}$ and *Trp53bp1*$^{-/-}$/*Atm*$^{-/-}$ cells (Table S2).

53BP1 suppresses chromosomal translocations in primary *Atm*$^{-/-}$ cells

To test the effect of persistent DSBs on translocation formation, we next quantified breaks and translocations in mitotic chromosomes of activated B cells. As expected (42), we observed an increased frequency of both spontaneous and IR-induced aberrations in all DNA repair-deficient mutants relative to wt controls (n=6 independent experiments; Fig. 4G–I, Table S3 for summary, Table S4 for individual experiments). Consistent with the lack of additional organismal phenotypes in growth and development (Fig. S1), the frequency of spontaneous breaks was similar in *Atm*$^{-/-}$ and *Trp53bp1*$^{-/-}$/*Atm*$^{-/-}$ B cells (Fig. 4G "mock"). In contrast, IR consistently induced an "excess" of chromosomal aberrations in *Trp53bp1*$^{-/-}$/*Atm*$^{-/-}$ cells relative to *Atm*$^{-/-}$ controls (n=6 independent experiments; n=0.5–3.2 "excess" breaks per cell (Fig. 4G "2 Gy"). When normalized to the *Atm*$^{-/-}$ control in the same stimulation, this difference was highly significant (p=0.009; Fig. 4H). The "excess" breaks were mostly "chromosome-type" (centrics and acentrics), consistent with their origin prior to replication (Fig. 4I). These observations were not specific to these experimental conditions, because we similarly observed an increase in the frequency of IR-induced aberrations in LPS-activated B cells (3.7 and 4.4 breaks/metaphase for *Atm*$^{-/-}$ and *Trp53bp1*$^{-/-}$/*Atm*$^{-/-}$ cells, respectively; Table S5) or in concanavalin A-activated T cells (3.0 and 3.4 breaks/metaphase for *Atm*$^{-/-}$ and *Trp53bp1*$^{-/-}$/*Atm*$^{-/-}$ cells, respectively; Table S6).

Consistent with the increased number of chromosomal breaks, we also observed an increase in the number of translocations in α-CD40/IL-4-activated double mutants (0.4, 1.0, 1.7 and 2.4 translocated ends per cell for wt, *Trp53bp1*$^{-/-}$, *Atm*$^{-/-}$ and *Trp53bp1*$^{-/-}$/*Atm*$^{-/-}$ metaphases, respectively; Table 2). Similar observations were made for LPS-activated B cells (Table 2). Finally, the greater number of breaks and translocations in double mutants was likely due to their defect in repair *per se*, because the marked G2/M checkpoint defect observed in *Atm*$^{-/-}$ cells was not modulated by 53BP1 status (Fig. S11).

53BP1 is dispensable for hybrid joint (HJ) formation, but suppresses large deletions at HJs

ATM suppresses the incorrect utilization of DNA ends during DSB repair (43). HJs are an aberrant product of V(D)J recombination, formed by the joining of a coding end to the signal end derived from the other participating gene segment. Consistent with its role in guiding appropriate end joining, ATM suppresses HJ formation (31). The role of 53BP1 in enforcing correct end utilization or in protecting DNA ends during short-range V(D)J recombination has not been addressed. We therefore assayed thymocytes from *Atm*$^{-/-}$ and *Trp53bp1*$^{-/-}$ mice for the presence of HJs as a measure of incorrect end utilization and examined the sequences of HJs for evidence of aberrant end processing and repair. Endogenous Dβ2-Vβ14 HJs were amplified from thymus DNA of 7 day-old wt, *Trp53bp1*$^{-/-}$, *Atm*$^{-/-}$ and *Trp53bp1*$^{-/-}$/*Atm*$^{-/-}$ mice (n=6 independent sets). Amplicons were detected by Southern hybridization to a radiolabeled, locus-specific probe (Fig. 5A). As expected, HJs were rare in wt thymocytes but readily detectable in *Atm*$^{-/-}$ cells (Fig. 5B, Fig. S12). In contrast, no or weak hybridization signals were observed in *Trp53bp1*$^{-/-}$ cells, indicating that, unlike ATM, 53BP1 does not function to suppress HJ formation.

Because previous work demonstrated that HJ formation in *Atm*$^{-/-}$ thymocytes is fully dependent on canonical NHEJ (44), we next asked whether 53BP1 is necessary for HJ formation in the absence of ATM. HJs were detected at similar amounts in *Trp53bp1*$^{-/-}$/*Atm*$^{-/-}$ and *Atm*$^{-/-}$ controls (Fig. 5B, Fig. S12A), suggesting that 53BP1 is dispensable for NHEJ-dependent repair in this context. However, while a single band of the expected size was observed in *Atm*$^{-/-}$ DNA, we consistently detected one or several additional lower molecular weight bands in *Trp53bp1*$^{-/-}$/*Atm*$^{-/-}$ samples (Fig. 5B and S12A). Sequencing of

gel-extracted, high-mobility bands confirmed the deletions (Fig. 5C–D, Fig. S12B–C), consistent with the interpretation that 53BP1 functions to protect a subset of DNA ends from extensive end-resection prior to HJ formation. Sequence analysis enabled us to distinguish independent events on the basis of differential N-region insertion. Incidentally, deletion endpoints appeared to cluster at two sites within the Dβ2 signal flank, residing 267 – 268 and 347 – 348 bp from the signal end (Fig. 5D). Moreover, an apparent bias toward deletion from the signal end was observed when recombinants were amplified with primers placed at similar distances from the coding or signal ends (Fig. S12B–C). Taken together, these observations indicate that, in the context of HJ formation in ATM-deficient cells, removal of 53BP1 does not affect the frequency of incorrect end utilization, but rather markedly increases the extent of end resection that accompanies the joining of a subset of incorrect ends.

Discussion

53BP1 is being increasingly recognized as a tumor suppressor in a wide range of human cancers (13–18). Significantly, its functions in NHEJ-mediated repair were previously reported to be epistatic with those of ATM (20), consistent with their mutual regulation (7, 20–24). Here, we find that their functional interaction in NHEJ is context-dependent. In this regard, we observe epistasis during organismal growth and development and in the suppression of spontaneous genomic instability. In contrast, we find that 53BP1 becomes limiting for NHEJ-mediated repair after IR or during oncogenic stress, when the load of DSBs per cell is greater. Importantly, this work demonstrates that, in the pro-oncogenic environment generated by ATM deficiency, even a modest aggravation of the NHEJ defect in the absence of 53BP1 may have a profound clinical effect. This observation is in keeping with a recent report that 53BP1 deficiency similarly cooperates with oncogenic stress associated with AID overexpression to suppress B cell lymphomagenesis (45).

The clonal RAG-dependent translocations that drive *Atm*$^{-/-}$ tumors are normally suppressed by NHEJ (31). We propose that the accelerated acquisition of these translocations in double mutants is a direct result of their greater defect in NHEJ. Although the number of TCRα/δ breaks detected by cytogenetics in *Atm*$^{-/-}$ and *Trp53bp1*$^{-/-}$/*Atm*$^{-/-}$ primary cells was too low for a direct comparison (our unpublished observations), we find that NHEJ-mediated repair in irradiated G1 splenocytes and thymocytes is consistently delayed in double mutants. When coupled with the severe checkpoint defects documented here, this deficiency alone could be sufficient to explain our observations in cycling cells, including: (1) increased numbers of γ-H2AX foci in G2; (2) increased polyploidy; and (3) increased chromosomal breaks and translocations in mitotic chromosomes. Our findings differ from those of a previous study which concluded that 53BP1 and ATM are fully epistatic in the repair of IR-induced DSB induced in G1 (20). This apparent discrepancy may reflect differences in methodologies, including but not limited to differential radiation dose and our use of ATM null cells rather than a chemical inhibitor of ATM.

Most relevant to our translocation-driven tumor model, we find a net increase in the formation of “random” chromosomal translocations in primary double mutant cells relative to single mutants. Although 53BP1 is required for the fusion of uncapped telomeres (9) and intra-chromosomal recombination (8, 46), 53BP1-deficient cells can nevertheless form intra- and inter-chromosomal rearrangements robustly (8, 45). In agreement with this notion, we find that approximately 30% of IR-induced chromosomal breaks are rearranged in 53BP1-deficient cells, regardless of ATM status. Intriguingly, the percentage of DNA ends undergoing translocation was higher (about 40%) in irradiated wild-type cells, despite the fact that they harbored fewer total breaks per cell and consequently fewer translocation “acceptors”. These observations suggest a model in which 53BP1 and ATM may play dual

roles in the context of translocations. In this model they would primarily function to suppress translocations by promoting appropriate rejoining of DSBs. However, if repair fails and DNA ends are dissociated, 53BP1 and/or ATM would promote “aberrant” repair to form translocations, perhaps by helping bring the ends together and/or promoting the recruitment of classical or alternative NHEJ factors (9, 24). The observed translocation frequency would then reflect the balance between their anti- and pro-translocation activities, a notion that will be further examined in future work.

Mechanistically, 53BP1 promotes NHEJ by suppressing inappropriate DNA end-resection (6–8, 23, 45, 47, 48), preventing large deletions and/or use of highly error-prone pathways (35). Previous work has shown that ATM regulates end-resection in 53BP1-deficient cells in a cell cycle-dependent manner (47). Specifically, ATM suppressed end-resection in 53BP1-deficient cells in G1, but not in S/G2 (6, 7). Consistent with these findings, we report here increased deletions in a subset of RAG-mediated HJs in 53BP1-deficient thymocytes also lacking ATM. Together with previous observations (6, 7), this finding suggests that formation of at least a subset of HJs (and possibly chromosomal translocations) may require cell cycle progression. However, our finding that sequences at coding, signal and hybrid joints in double mutants are consistent with ligase IV-dependent canonical NHEJ suggests that this may be nevertheless the main pathway mediating HJs and chromosomal translocations, a notion that will be further examined in future work.

Finally, this work has important implications for our understanding of cancers harboring genetic alterations in DDR factors. Given that mutations in ATM are common in human cancers, it will be interesting to determine whether they are non-mutually exclusive with 53BP1 mutations, and to define their interplay in the natural history of disease and the response to therapy.

Supplementary Material

Refer to Web version on PubMed Central for supplementary material.

Acknowledgments

Financial support: Sonia Franco was supported by Research Scholar Grant RSG-12-160-01-DMC from the American Cancer Society. Stephen Desiderio was supported by grants CA016519 and CA160256 from the National Cancer Institute and by a gift to the Institute for Cell Engineering.

References

1. Harper JW, Elledge SJ. The DNA damage response: ten years after. Molecular cell. 2007; 28:739–45. [PubMed: 18082599]
2. Jackson SP, Bartek J. The DNA-damage response in human biology and disease. Nature. 2009; 461:1071–8. [PubMed: 19847258]
3. Matsuoka S, Ballif BA, Smogorzewska A, McDonald ER 3rd, Hurov KE, Luo J, et al. ATM and ATR substrate analysis reveals extensive protein networks responsive to DNA damage. Science. 2007; 316:1160–6. [PubMed: 17525332]
4. Al-Hakim A, Escribano-Diaz C, Landry MC, O’Donnell L, Panier S, Szilard RK, et al. The ubiquitous role of ubiquitin in the DNA damage response. DNA repair. 2010; 9:1229–40. [PubMed: 21056014]
5. Noon AT, Goodarzi AA. 53BP1-mediated DNA double strand break repair: Insert bad pun here. DNA repair. 2011; 10:1071–6. [PubMed: 21868291]
6. Bothmer A, Robbiani DF, Feldhahn N, Gazumyan A, Nussenzweig A, Nussenzweig MC. 53BP1 regulates DNA resection and the choice between classical and alternative end joining during class

switch recombination. The Journal of experimental medicine. 2010; 207:855–65. [PubMed: 20368578]

7. Bunting SF, Callen E, Wong N, Chen HT, Polato F, Gunn A, et al. 53BP1 inhibits homologous recombination in Brca1-deficient cells by blocking resection of DNA breaks. Cell. 2010; 141:243–54. [PubMed: 20362325]
8. Difilippantonio S, Gapud E, Wong N, Huang CY, Mahowald G, Chen HT, et al. 53BP1 facilitates long-range DNA end-joining during V(D)J recombination. Nature. 2008; 456:529–33. [PubMed: 18931658]
9. Dimitrova N, Chen YC, Spector DL, de Lange T. 53BP1 promotes non-homologous end joining of telomeres by increasing chromatin mobility. Nature. 2008
10. Halazonetis TD, Gorgoulis VG, Bartek J. An oncogene-induced DNA damage model for cancer development. Science. 2008; 319:1352–5. [PubMed: 18323444]
11. Lavin MF. Ataxia-telangiectasia: from a rare disorder to a paradigm for cell signalling and cancer. Nat Rev Mol Cell Biol. 2008; 9:759–69. [PubMed: 18813293]
12. Skowronska A, Parker A, Ahmed G, Oldreive C, Davis Z, Richards S, et al. Biallelic ATM Inactivation Significantly Reduces Survival in Patients Treated on the United Kingdom Leukemia Research Fund Chronic Lymphocytic Leukemia 4 Trial. Journal of clinical oncology : official journal of the American Society of Clinical Oncology. 2012
13. Bouwman P, Aly A, Escandell JM, Pieterse M, Bartkova J, van der Gulden H, et al. 53BP1 loss rescues BRCA1 deficiency and is associated with triple-negative and BRCA-mutated breast cancers. Nature structural & molecular biology. 2010; 17:688–95.
14. Li X, Xu B, Moran MS, Zhao Y, Su P, Haffty BG, et al. 53BP1 functions as a tumor suppressor in breast cancer via the inhibition of NF-kappaB through miR-146a. Carcinogenesis. 2012; 33:2593–600. [PubMed: 23027628]
15. Neboori HJ, Haffty BG, Wu H, Yang Q, Aly A, Goyal S, et al. Low p53 binding protein 1 (53BP1) expression is associated with increased local recurrence in breast cancer patients treated with breast-conserving surgery and radiotherapy. International journal of radiation oncology, biology, physics. 2012; 83:e677–83.
16. Squatrito M, Vanoli F, Schultz N, Jasin M, Holland EC. 53BP1 Is a Haploinsufficient Tumor Suppressor and Protects Cells from Radiation Response in Glioma. Cancer research. 2012; 72:5250–60. [PubMed: 22915756]
17. Takeyama K, Monti S, Manis JP, Dal Cin P, Getz G, Beroukhim R, et al. Integrative analysis reveals 53BP1 copy loss and decreased expression in a subset of human diffuse large B-cell lymphomas. Oncogene. 2008; 27:318–22. [PubMed: 17637749]
18. Jaspers JE, Kersbergen A, Boon U, Sol W, van Deemter L, Zander SA, et al. Loss of 53BP1 causes PARP inhibitor resistance in Brca1-mutated mouse mammary tumors. Cancer discovery. 2013; 3:68–81. [PubMed: 23103855]
19. Lee JH, Goodarzi AA, Jeggo PA, Paull TT. 53BP1 promotes ATM activity through direct interactions with the MRN complex. The EMBO journal. 2010; 29:574–85. [PubMed: 20010693]
20. Noon AT, Shibata A, Rief N, Lobrich M, Stewart GS, Jeggo PA, et al. 53BP1-dependent robust localized KAP-1 phosphorylation is essential for heterochromatic DNA double-strand break repair. Nature cell biology. 2010; 12:177–84.
21. Chapman JR, Barral P, Vannier JB, Borel V, Steger M, Tomas-Loba A, et al. RIF1 Is Essential for 53BP1-Dependent Nonhomologous End Joining and Suppression of DNA Double-Strand Break Resection. Molecular cell. 2013
22. Escribano-Diaz C, Orthwein A, Fradet-Turcotte A, Xing M, Young JT, Tkac J, et al. A Cell Cycle-Dependent Regulatory Circuit Composed of 53BP1-RIF1 and BRCA1-CtIP Controls DNA Repair Pathway Choice. Molecular cell. 2013
23. Di Virgilio M, Callen E, Yamane A, Zhang W, Jankovic M, Gitlin AD, et al. Rif1 Prevents Resection of DNA Breaks and Promotes Immunoglobulin Class Switching. Science. 2013
24. Zimmermann M, Lottersberger F, Buonomo SB, Sfeir A, de Lange T. 53BP1 Regulates DSB Repair Using Rif1 to Control 5′ End Resection. Science. 2013

25. Feng L, Fong KW, Wang J, Wang W, Chen J. RIF1 Counteracts BRCA1-mediated End Resection during DNA Repair. The Journal of biological chemistry. 2013; 288:11135–43. [PubMed: 23486525]
26. Ward IM, Minn K, van Deursen J, Chen J. p53 Binding protein 53BP1 is required for DNA damage responses and tumor suppression in mice. Molecular and cellular biology. 2003; 23:2556–63. [PubMed: 12640136]
27. Borghesani PR, Alt FW, Bottaro A, Davidson L, Aksoy S, Rathbun GA, et al. Abnormal development of Purkinje cells and lymphocytes in Atm mutant mice. Proceedings of the National Academy of Sciences of the United States of America. 2000; 97:3336–41. [PubMed: 10716718]
28. Orsburn B, Escudero B, Prakash M, Gesheva S, Liu G, Huso DL, et al. Differential requirement for H2AX and 53BP1 in organismal development and genome maintenance in the absence of poly(ADP)ribosyl polymerase 1. Molecular and cellular biology. 2010; 30:2341–52. [PubMed: 20231360]
29. Rybanska I, Ishaq O, Chou J, Prakash M, Bakhsheshian J, Huso DL, et al. PARP1 and DNA-PKcs synergize to suppress p53 mutation and telomere fusions during T-lineage lymphomagenesis. Oncogene. 2012
30. Zhang L, Reynolds TL, Shan X, Desiderio S. Coupling of v(d)j recombination to the cell cycle suppresses genomic instability and lymphoid tumorigenesis. Immunity. 2011; 34:163–74. [PubMed: 21349429]
31. Bredemeyer AL, Sharma GG, Huang CY, Helmink BA, Walker LM, Khor KC, et al. ATM stabilizes DNA double-strand-break complexes during V(D)J recombination. Nature. 2006; 442:466–70. [PubMed: 16799570]
32. Jazayeri A, Falck J, Lukas C, Bartek J, Smith GC, Lukas J, et al. ATM- and cell cycle-dependent regulation of ATR in response to DNA double-strand breaks. Nature cell biology. 2006; 8:37–45.
33. Liyanage M, Weaver Z, Barlow C, Coleman A, Pankratz DG, Anderson S, et al. Abnormal rearrangement within the alpha/delta T-cell receptor locus in lymphomas from Atm-deficient mice. Blood. 2000; 96:1940–6. [PubMed: 10961898]
34. Zha S, Bassing CH, Sanda T, Brush JW, Patel H, Goff PH, et al. ATM-deficient thymic lymphoma is associated with aberrant tcrd rearrangement and gene amplification. The Journal of experimental medicine. 2010; 207:1369–80. [PubMed: 20566716]
35. Symington LS, Gautier J. Double-strand break end resection and repair pathway choice. Annual review of genetics. 2011; 45:247–71.
36. Marculescu R, Vanura K, Montpellier B, Roulland S, Le T, Navarro JM, et al. Recombinase, chromosomal translocations and lymphoid neoplasia: targeting mistakes and repair failures. DNA repair. 2006; 5:1246–58. [PubMed: 16798110]
37. Callen E, Jankovic M, Difilippantonio S, Daniel JA, Chen HT, Celeste A, et al. ATM prevents the persistence and propagation of chromosome breaks in lymphocytes. Cell. 2007; 130:63–75. [PubMed: 17599403]
38. Callen E, Jankovic M, Wong N, Zha S, Chen HT, Difilippantonio S, et al. Essential role for DNA-PKcs in DNA double-strand break repair and apoptosis in ATM-deficient lymphocytes. Molecular cell. 2009; 34:285–97. [PubMed: 19450527]
39. Franco S, Murphy MM, Li G, Borjeson T, Boboila C, Alt FW. DNA-PKcs and Artemis function in the end-joining phase of immunoglobulin heavy chain class switch recombination. The Journal of experimental medicine. 2008; 205:557–64. [PubMed: 18316419]
40. Gordon DJ, Resio B, Pellman D. Causes and consequences of aneuploidy in cancer. Nature reviews Genetics. 2012; 13:189–203.
41. Weston VJ, Oldreive CE, Skowronska A, Oscier DG, Pratt G, Dyer MJ, et al. The PARP inhibitor olaparib induces significant killing of ATM-deficient lymphoid tumor cells in vitro and in vivo. Blood. 2010; 116:4578–87. [PubMed: 20739657]
42. Franco S, Gostissa M, Zha S, Lombard DB, Murphy MM, Zarrin AA, et al. H2AX prevents DNA breaks from progressing to chromosome breaks and translocations. Molecular cell. 2006; 21:201–14. [PubMed: 16427010]
43. Bennardo N, Stark JM. ATM limits incorrect end utilization during non-homologous end joining of multiple chromosome breaks. PLoS genetics. 2010; 6:e1001194. [PubMed: 21079684]

44. Bredemeyer AL, Huang CY, Walker LM, Bassing CH, Sleckman BP. Aberrant V(D)J recombination in ataxia telangiectasia mutated-deficient lymphocytes is dependent on nonhomologous DNA end joining. J Immunol. 2008; 181:2620–5. [PubMed: 18684952]

45. Jankovic M, Feldhahn N, Oliveira TY, Silva IT, Kieffer-Kwon KR, Yamane A, et al. 53BP1 Alters the Landscape of DNA Rearrangements and Suppresses AID-Induced B Cell Lymphoma. Molecular cell. 2013

46. Bothmer A, Robbiani DF, Di Virgilio M, Bunting SF, Klein IA, Feldhahn N, et al. Regulation of DNA End Joining, Resection, and Immunoglobulin Class Switch Recombination by 53BP1. Molecular cell. 2011; 42:319–29. [PubMed: 21549309]

47. Yamane A, Robbiani DF, Resch W, Bothmer A, Nakahashi H, Oliveira T, et al. RPA Accumulation during Class Switch Recombination Represents 5′-3′ DNA-End Resection during the S-G2/M Phase of the Cell Cycle. Cell reports. 2013

48. Sfeir A, de Lange T. Removal of shelterin reveals the telomere end-protection problem. Science. 2012; 336:593–7. [PubMed: 22556254]

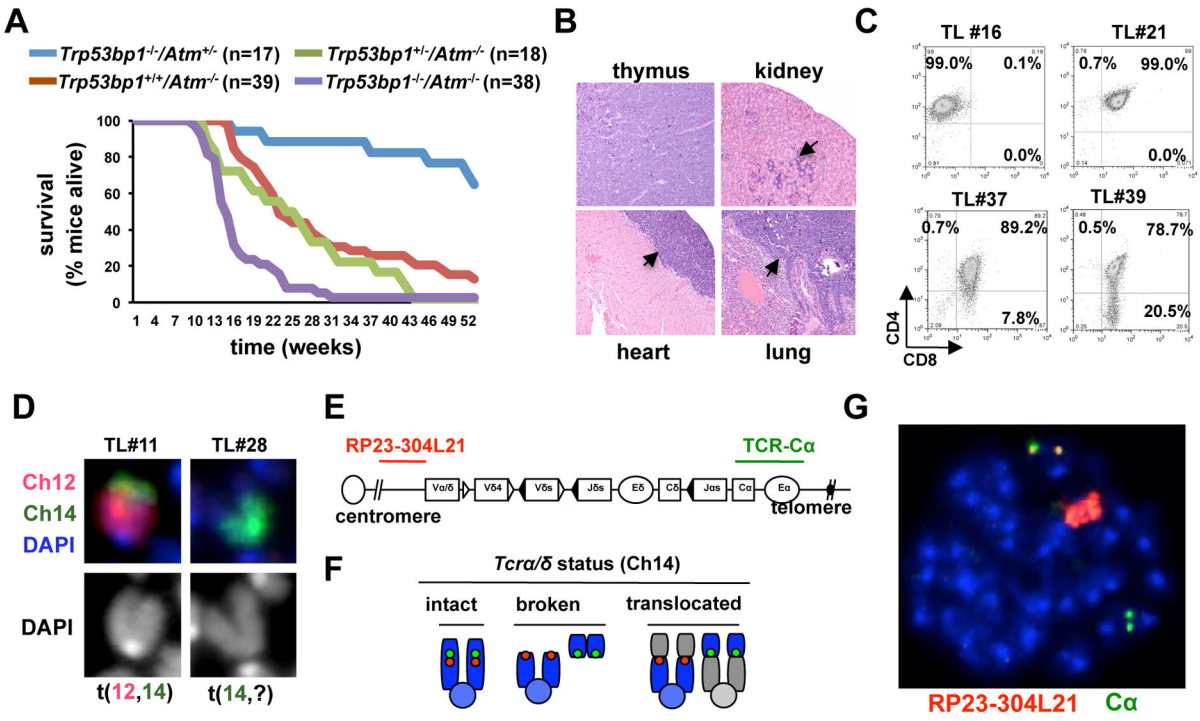

Fig. 1.

53BP1 deficiency accelerates thymic lymphomagenesis in *Atm*$^{-/-}$ mice. A, survival (Kaplan Meier) curves of *Trp53bp1*$^{-/-}$/*Atm*$^{-/-}$ and control mice. B, moribund *Trp53bp1*$^{-/-}$/*Atm*$^{-/-}$ mice were euthanized and organs stained with hematoxilin and eosin (H/E). Thymus architecture was effaced by lymphoma growth. Black arrows point to lymphoblasts infiltrating the kidney, epicardium and lung parenchyma. C, immunophenotyping of *Trp53bp1*$^{-/-}$/*Atm*$^{-/-}$ tumor cells after staining with antibodies to CD4 and CD8. D, examples of clonal chromosomal rearrangements involving chromosome 14 in *Trp53bp1*$^{-/-}$/*Atm*$^{-/-}$ tumor cells using chromosome paints. E, schematic of the TCRα/δ locus in mouse chromosome 14 and location of BAC probes (not to scale). F, read-out of FISH assay; G, representative example of a *Trp53bp1*$^{-/-}$/*Atm*$^{-/-}$ tumor metaphase showing “split” BAC signals and massive amplification of the 5′ probe (red).

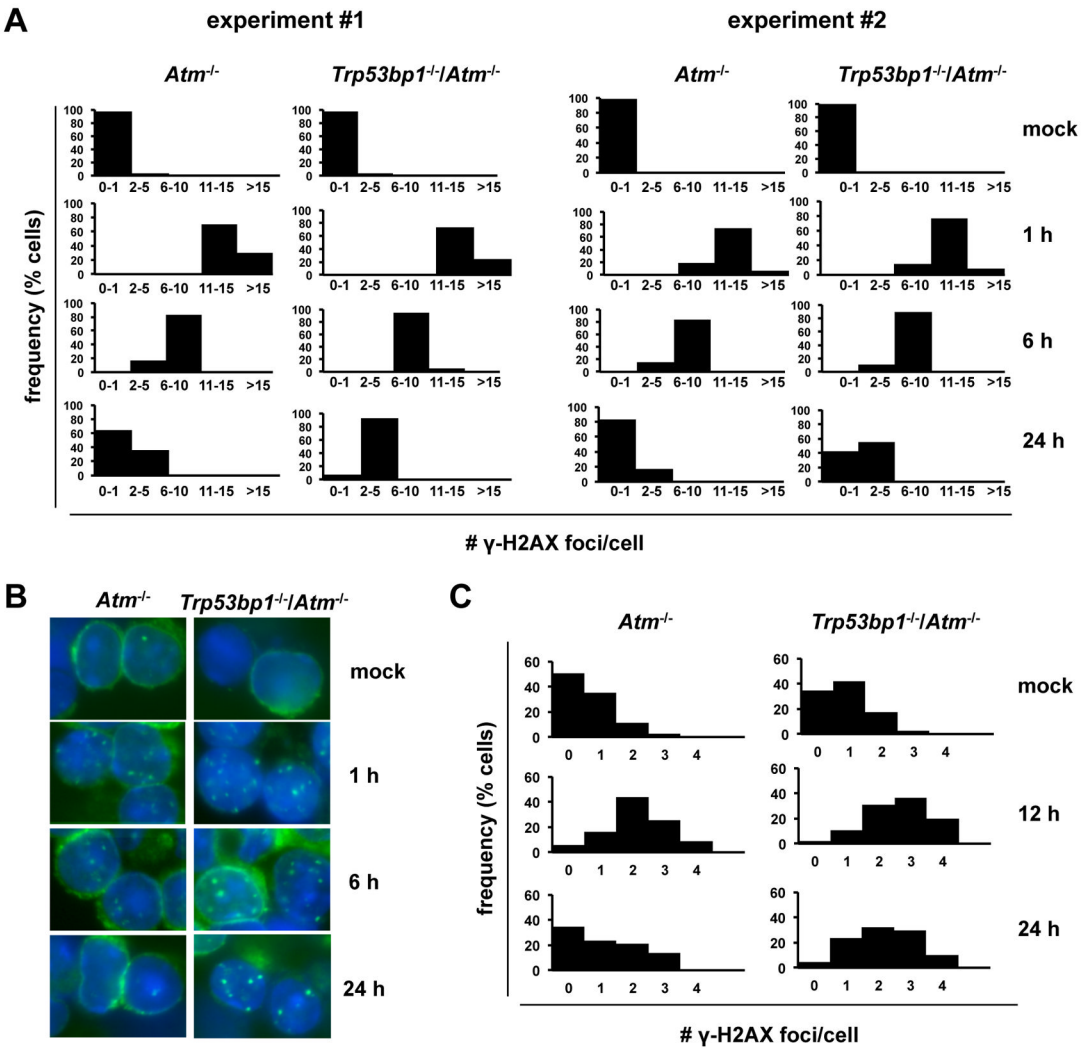

Fig. 2.

53BP1 deficiency aggravates the NHEJ defect in primary $Atm^{-/-}$ cells. A, cells were irradiated and the number of γ-H2AX foci per nucleus quantified by indirect immunofluorescence. N=100 cells per histogram. B, representative examples of cells in A. C, mice were irradiated, allowed to repair *in vivo* and euthanized at the indicated timepoints. The number of γ-H2AX foci per nucleus was quantified in thymus cryosections by indirect immunofluorescence. N=150 cells per histogram.

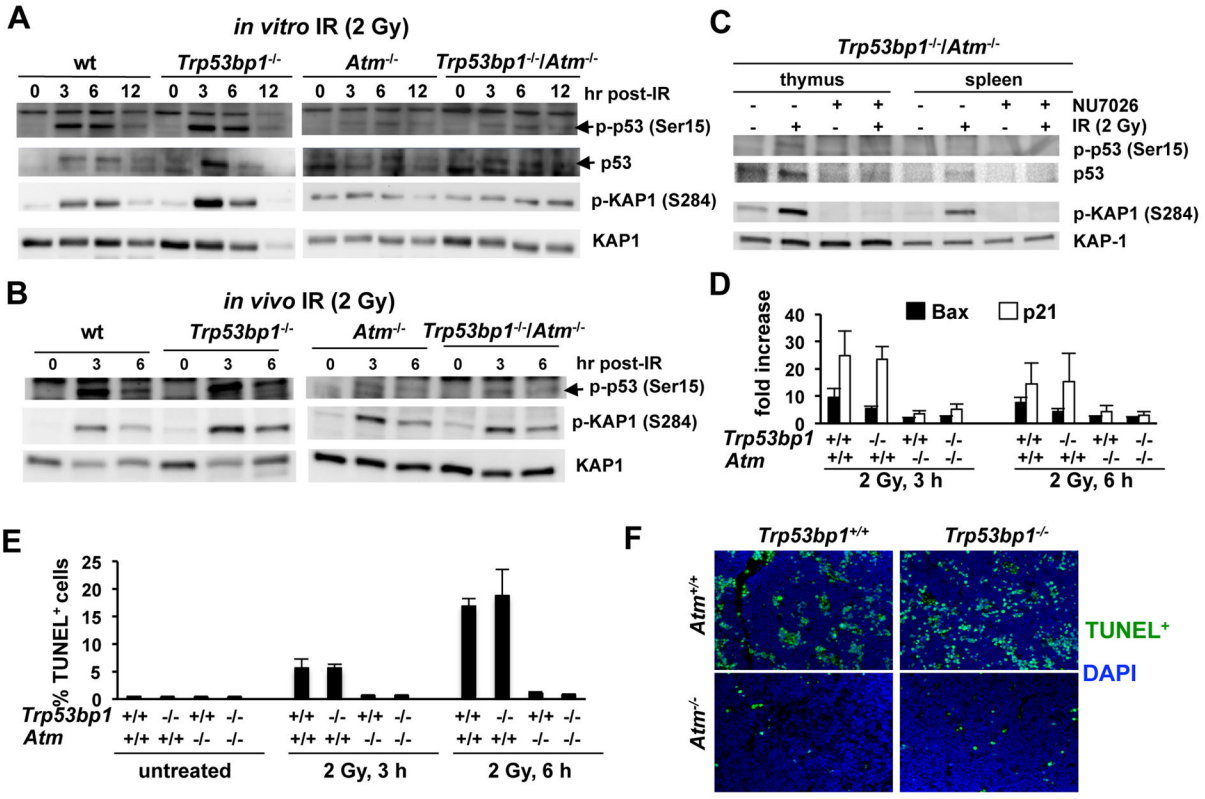

Fig. 3.

Effect of 53BP1 deficiency on the ATM/p53 axis function. A, thymocytes were irradiated *in vitro* and harvested at the indicated timepoints for immunoblotting. Total KAP1 serves as loading control. B, mice were irradiated, allowed to repair *in vivo* and euthanized at the indicated timepoints. Thymocytes were analyzed as in A. C, *Trp53bp1*$^{-/-}$/*Atm*$^{-/-}$ thymocytes were irradiated in the presence or absence of the DNA-PKcs inhibitor NU7026 and harvested at 3 hours for immunoblotting. D–F, mice were irradiated and euthanized at either 3 or 6 hours post-IR. D, thymus RNA was reverse transcribed and p21 or Bax cDNA amplified by Real-Time RT-PCR. E–F, apoptosis was quantified in thymic sections using the TUNEL assay. Representative examples are shown in F. Bars represent the average and standard deviation of 3 experiments.

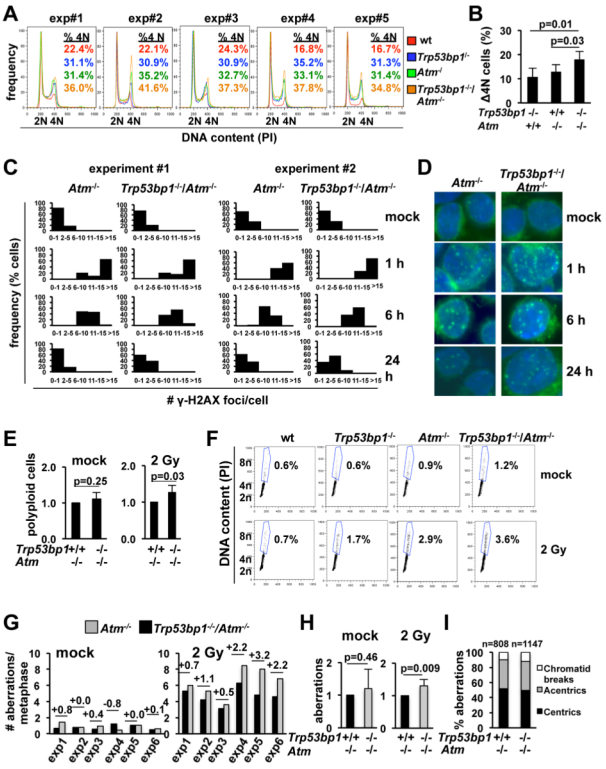

Fig. 4.

53BP1 deficiency increases the number of chromosomal translocations in irradiated *Atm*$^{-/-}$ primary cells. A, α-CD40/IL-4-activated B cells were irradiated, allowed to repair for 24 hours and stained with propidium iodide (PI) for analysis of cell cycle distribution. B, increase in the number of cells with 4N DNA content 24 hours after IR, relative to wt cells in the same experiment. Bars represent the average and standard deviation of the 5 experiments in A. C, distribution of the number of γ-H2AX foci per nucleus. N=100 cells per histogram. D, representative microphotographs of cells in C. E, frequency of cells with >4N DNA content 24 hr after IR. Data for the *Trp53bp1*$^{-/-}$/*Atm*$^{-/-}$ culture was normalized to the *Atm*$^{-/-}$ control in the same experiment. Bars represent the average and standard deviation of 5 mice per genotype in 5 independent experiments. F, representative FACs plots of E. G, quantification of the number of chromosomal breaks 24 hours after IR using telomere FISH. H, the frequency of chromosomal breaks per metaphase in *Trp53bp1*$^{-/-}$/*Atm*$^{-/-}$ cultures was normalized to *Atm*$^{-/-}$ cultures in the same experiment. Bars represent the average and standard deviation of 6 mice per genotype in 6 independent experiments. I, chromosomal breaks in G were classified as “chromosome-type” (centric and acentric chromosomes) or “chromatid-type”. The total number of aberrations analyzed is indicated.

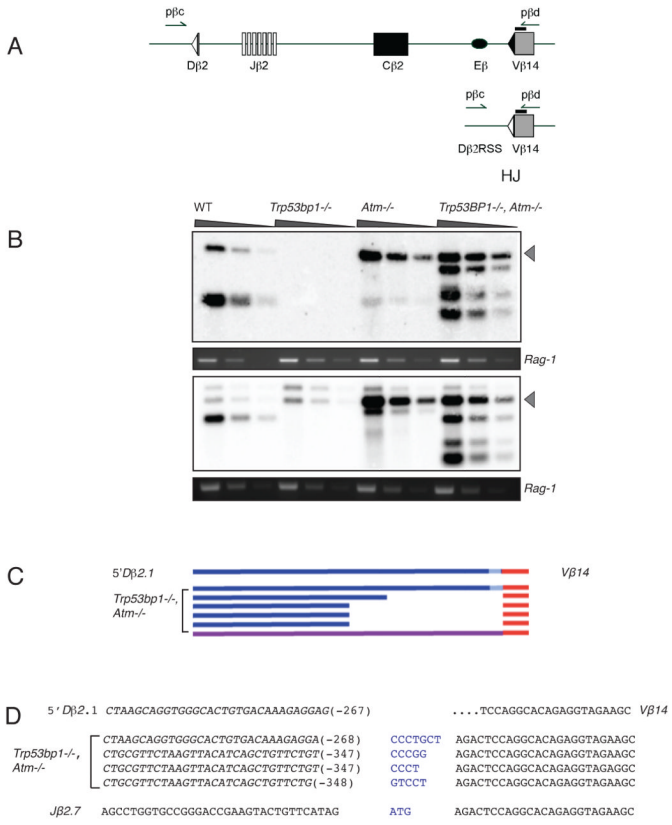

Fig. 5.

Deletions at hybrid V(D)J recombination junctions in *Trp53bp1*$^{-/-}$/*Atm*$^{-/-}$ mice. A, a portion of the mouse *TCRβ* locus prior to (top panel) and following (bottom panel) formation of a hybrid joint between *Dβ2* and *Vβ14*. Arrows indicate position of PCR primers. For simplicity, only the inside pair of a nested PCR primer set is depicted. Black bar indicates location of hybridization probe. B, detection of *Dβ2-Vβ14* hybrid joints in thymic genomic DNA. Grey arrowhead, expected size of an intact hybrid junction product (870 bp). A portion of the *Rag-1* gene was amplified in parallel as a loading control. Six mice of each genotype were assayed; representative data for two mice are shown. C, schematic diagram of aberrant hybrid joints from *Trp53bp1*$^{-/-}$/*Atm*$^{-/-}$ mice. Products migrating with higher mobility than intact hybrid junctions were excised, cloned and sequenced (see Methods). D, examples of nucleotide sequences across aberrant hybrid junctions from *Trp53bp1*$^{-/-}$/*Atm*$^{-/-}$ mice. Top line, germline *Vβ14* sequence. Lines 2–5 below, recombinant junctions; n additions are indicated in blue and length of deletions are indicated in parentheses. Bottom line, one clone contained a sequence in which the *Jβ2.7* gene segment is aberrantly rejoined to *Vβ14*.

Table 1

Analysis of *Trp53bp1*$^{-/-}$/*Atm*$^{-/-}$ and control *Atm*$^{-/-}$ and *Trp53bp1*$^{+/-}$/*Atm*$^{-/-}$ thymic lymphomas

Mouse ID	Genotype	Gender	Age at death (weeks)	Tumor CD4/CD8 labeling[a]	Chromosome paint analysis		# chromosomes/ cell (range) [b]
					chrom 14 abnormalities (% metaphases)	chrom 12 abnormalities (% metaphases)	
M#4	*Atm*$^{-/-}$	F	16.5	DP	n.d.	n.d.	n.d.
M#36	*Atm*$^{-/-}$	F	16	CD4 SP	n.d.	n.d.	n.d.
M#30	*Atm*$^{-/-}$	F	23	DP	Yes (98%)	Yes (98%)	41.7 ± 0.5 (41–42)
M#35	*Atm*$^{-/-}$	M	24	DP	Yes (100%)	Yes (100%)	40.0 ± 0.0 (40-40)
M#2	*Trp53bp1*$^{+/-}$/*Atm*$^{-/-}$	M	12	DP	n.d.	n.d.	n.d.
M#5	*Trp53bp1*$^{+/-}$/*Atm*$^{-/-}$	F	18	DP/DN	n.d.	n.d.	n.d.
M#49	*Trp53bp1*$^{+/-}$/*Atm*$^{-/-}$	M	12	DP/CD4 SP	n.d.	n.d.	n.d.
M#10	*Trp53bp1*$^{+/-}$/*Atm*$^{-/-}$	F	27	DP/CD4 SP	n.d.	n.d.	n.d.
M#70	*Trp53bp1*$^{+/-}$/*Atm*$^{-/-}$	M	14	DP	n.d.	n.d.	n.d.
M#11	*Trp53bp1*$^{-/-}$/*Atm*$^{-/-}$	M	14.5	DP	Yes (96%)	Yes (98%)	39.8 ± 0.4 (39–40)
M#16	*Trp53bp1*$^{-/-}$/*Atm*$^{-/-}$	M	15	CD4 SP	Yes (96%)	No	41.7 ± 103 (38–44)
M#21	*Trp53bp1*$^{-/-}$/*Atm*$^{-/-}$	M	16.5	DP	Yes (100%)	Yes (100%)	40.8 ± 0.6 (40–42)
M#28	*Trp53bp1*$^{-/-}$/*Atm*$^{-/-}$	M	16	DP	Yes (98%)	Yes (94%)	40.1 ± 0.6 (39–41)
M#37	*Trp53bp1*$^{-/-}$/*Atm*$^{-/-}$	M	14	DP	Yes (100%)	Yes (100%)	40.0 ± 0.5 (39–41)
M#39	*Trp53bp1*$^{-/-}$/*Atm*$^{-/-}$	M	13.5	DP/CD8 SP	Yes (92%)	Yes (92%)	40.0 ± 0.2 (40–41)

[a] DP, double positive for CD4 and CD8; SP, single positive; mixed populations were observed in some tumors, as indicated.

[b] average and standard deviation; n=20–30 metaphases per tumor; n.d., not done.

Table 2

Analysis of genomic stability in irradiated (2 Gy) B cells deficient for 53BP1 and/or ATM. Metaphases were obtained 24 hr after exposure to IR and stained with a telomere probe. N=3 mice per genotype

Genotype	Cytokine	# metaphases analyzed	# broken ends analyzed	#translocated ends/ #nontranslocated ends	%trasnlocated ends/%nontranslocated ends	# breaks per cell/# translocated breaks per cell	ratio translocated/nontranslocated
wt	α-CD40/IL-4	90	91	37/54	40.7/59.3	1.0/0.4	0.7
Trp53bp1$^{-/-}$	α-CD40/IL-4	90	301	93/208	30.9/69.1	3.3/1.0	0.4
Atm$^{-/-}$	α-CD40/IL-4	90	471	150/321	31.8/68.2	5.2/1.7	0.5
Trp53bp1$^{-/-}$/*Atm*$^{-/-}$	α-CD40/IL-4	90	741	220/521	29.7/70.3	8.2/2.4	0.4
wt	LPS	90	82	33/49	40.2/59.8	0.9/0.4	0.7
Trp53bp1$^{-/-}$	LPS	90	207	44/163	21.3/78.7	2.3/0.5	0.3
Atm$^{-/-}$	LPS	90	332	99/233	29.8/70.2	3.7/1.1	0.4
Trp53bp1$^{-/-}$/*Atm*$^{-/-}$	LPS	90	392	121/271	30.9/69.1	4.4/1.3	0.4